Le T.D.H., Bonani W., Speranza G., Sglavo V., Ceccato R., Maniglio D., Motta A., Migliaresi C.
Processing and characterization of diatom nanoparticles and microparticles as potential source of silicon for bone tissue engineering, Materials Science and Engineering C, 59, 471–479, 2016
10.1016/j.msec.2015.10.040

Processing and Characterization of Diatom Nanoparticles and Microparticles as Potential Source of Silicon for Bone Tissue Engineering

Thi Duy Hanh Le[1,2], Walter Bonani[1,2,3], Giorgio Speranza[4], Vincenzo Sglavo[1], Riccardo Ceccato[1], Devid Maniglio[1,2,3], Antonella Motta[1,2,3], Claudio Migliaresi[1,2,3]

[1] Department of Industrial Engineering, University of Trento, Trento, Italy
[2] BIOtech Research Center and European Institute of Excellence on Tissue Engineering and Regenerative Medicine, Trento, Italy
[3] Interuniversity Consortium for Science and Technology of Materials, Trento Research Unit, Trento, Italy
[4] Center for Materials and Microsystems, PAM-SE, Fondazione Bruno Kessler, Trento, Italy

Corresponding author:

Professor Claudio Migliaresi
Department of Industrial Engineering and BIOtech Research Center, University of Trento, Via Sommarive 9, 38123. Trento, Italy

Email: claudio.migliaresi@unitn.it

Abstract

Silicon plays an important role in bone formation and maintenance, improving osteoblast cell function and inducing mineralization. Often, bone deformation and long bone abnormalities have been associated with silica/silicon deficiency. Diatomite, a natural deposit of diatom skeleton, is a cheap and abundant source of biogenic silica. The aim of the present study is to validate the potential of diatom particles derived from diatom skeletons as silicon-donor materials for bone tissue engineering applications. Raw diatomite (RD) and calcined diatomite (CD) powders were purified by acid treatments, and diatom microparticles (MPs) and nanoparticles (NPs) were produced by fragmentation of purified diatoms under alkaline conditions. The influence of processing on the surface chemical composition of purified diatomites was evaluated by X-ray photoelectron spectroscopy (XPS). Diatoms NPs were also characterized in terms of morphology and size distribution by transmission electron microscopy (TEM) and dynamic light scattering (DLS), whilst diatom MPs morphology was analyzed by scanning electron microscopy (SEM). Surface area and microporosity of the diatom particles were evaluated by nitrogen physisorption methods. Release of silicon ions from diatom-derived particles was demonstrated using inductively coupled plasma optical emission spectrometry (ICP/OES); furthermore, silicon release kinetic was found to be influenced by diatomite purification method and particle size. Diatom-derived microparticles (MPs) and nanoparticles (NPs) showed limited or no cytotoxic effect in vitro depending on the administration conditions.

Keywords: Silica, diatomite, diatom nanoparticles, silicon release, bone regeneration.

Abbreviations

RD: Raw diatomite powder

CD: Calcined diatomite powder

AD: Acid-purified raw diatomite powder

CAD: Acid-purified calcined diatomite powder

D-MPs: Diatom microparticles

D-NPs: Diatom nanoparticles

XPS: X-ray photoelectron spectroscopy

TEM : Transmission electron microscopy

SAED: Selected area (electron) diffraction

SEM : Scanning electron microscopy

ICP: Inductively coupled plasma

EDAX : Energy dispersive X-ray analysis

DLS: Dynamic light scattering

1. Introduction

Silicon is the main component of silica formed exo- and endo-skeletons in some marine organisms [1]. The skeleton of unicellular marine organisms such as sea sponges and diatoms consists of hydrated amorphous silica which is gradually formed by immobilization and internalization of monosilicic acid in a process addressed as biosilicification [2]–[4].

Nevertheless, silicon is also involved in the biomineralization processes in mammals. Calcification involves many stages including formation of calcium phosphate under the direct regulatory control of several biological systems and in presence of elemental traces such as silicon, zinc and magnesium [5]–[7]. Silicon is believed to be an essential element for bone development, although its role is not completely understood [8], [9]. For instance, silicon has been associate with the precipitation of calcium phosphate in the early stage of bone mineralization [7], [10]. In addition, the presence of silicon at the inorganic/organic interface regulates the interaction between collagen and proteoglycans improving the quality of the extracellular matrix (ECM) [11]. Silicon can induce stem cell differentiation in osteoblasts and osteocytes [12]–[14]; furthermore, silicon directly inhibits osteoclast formation and bone resorption [15].

Use of degradable amorphous silica particles has been proposed to improve mineralization in bone regeneration applications besides other inorganic materials such as hydroxylapatite, tri-calcium phosphate, glass ceramic or zirconia [16], [17]. However, bioactivity of particles significantly depends on size, shape and surface properties [18]–[21]. Recent studies have been focused on possible applications of amorphous silica nanoparticles as dietary supplement for bone regeneration [22], [23]. Additionally, silica has been successfully incorporated with hydroxylapatite to enhance osteoconductivity of scaffolds for bone tissue regeneration [24], [25]. Silk or collagen scaffolds loaded with amorphous silica particles have been successfully proposed to improve osteoinductivity [26]–[28]. So far a variety of amorphous silica sources have been considered. Often silica particles are of synthetic origin and are produced using chemicals and surfactants whose residues might have toxic effects [18], [29]. So, there is a quest for abundant and reliable alternative sources of amorphous silica.

Diatomite, also known as diatomaceous earth, is the marine sediment of silica diatom skeleton remains. Diatomite is an inexpensive and unlimited source of biogenic silica. Thanks to their peculiar morphology and porosity, diatom skeletons derived from diatomite have been proposed for uses in photonics, drug delivery and molecular catalysis applications [30]–[33]. We think that diatomite could be a promising natural source of amorphous silica also for bone tissue engineering applications. Biomedical uses of biogenic silica have been

preconized by Wang et al. [2], but to date diatomite-derived silica particles have never been used as a part of tissue engineering scaffolds. We think that diatom microparticles and nanoparticles be useful as bioactive silicon-donor additives for degradable engineered scaffolds and bone defect fillers following the silicon role on bone mineralization.

However, raw diatomite contains some local contaminations such as clays and other inorganic and organic compounds that require purification before any medical use and the yield of diatomite purification processes depend on diatom type and source [34].

Here, raw diatomite (RD) and calcined diatomite (CD) powders were purified in strong acid conditions, and diatom nanoparticles (NPs) and microparticles (MPs) were subsequently produced by treating the skeletons in alkaline solution. NPs and MPs morphology, elemental composition and specific surface area were determined. Silicon ion released by diatom particles dissolution has been evaluated with dissolution experiments and cytotoxicity tests of diatom particles have been performed.

2. Materials and Methods

2.1 Materials

Powder form of raw diatomite materials (RD) used in this study was provided by Phu Yen mineral joint stock company (Phu Yen province, Viet Nam). RD powder was passed through a metallic sieve (mesh size 250 µm) to remove aggregates and macroscopic contaminations.

Phosphate buffer solution (PBS), sodium hydroxide (NaOH), hydrochloric acid (HCl) and Triton X-100 were purchase from Sigma-Aldrich (St. Louis, MO, USA). All reagents and solvents were used as received without further purification.

2.2 Raw diatomite purifications

2.2.1 Acid-purified raw diatomite powder

RD powder underwent acid treatment to remove inorganic contaminations; purification protocol modified from [35]. Briefly, RD powder was dried overnight in oven at 102ºC, passed through a metallic sieve (mesh size 125 µm) to remove larger aggregates, and then acid-treated with 1M HCl solution at 55ºC (in the proportion of 100 mg of powder per ml of HCl solution) for 24 hours under continuous stirring to remove the inorganic contamination**.** Afterwards, the obtained slurry was concentrated with a paper filter; the remaining solid part was washed and allowed to sediment in deionized water (DI water) for at least 10 times. Finally, the sediment was dried in oven at 102ºC and sieved through a 63 µm pore size sieve to obtain acid-purified RD (hereinafter AD) consisting of single diatoms.

2.2.2 Acid-purified calcined diatomite powder

In this case, raw diatomite powder (RD) was heated at 650ºC in air for 3 hours to reduce organic contaminations [36]. Calcined diatomite powder (CD) was then passed through a metallic sieve (mesh size 125 µm), then treated with acid as explained before to obtain acid-purified CD (hereinafter named CAD).

2.3 Diatom microparticles and nanoparticles from purified diatoms

Diatom microparticles and nanoparticles were produced from purified diatoms powders (both AD and CAD) by mechanical fragmentation in alkaline conditions [37], [38]. Briefly, AD and CAD powders were suspended in 0.1M NaOH solution (typically, 10 mg of diatomite powder per ml of alkaline solution was used), and suspension was vigorously stirred for 2 weeks at room temperature (RT) to break diatoms. Afterward, the alkaline suspension was kept at RT for one week to allow for sedimentation.

The unsettled colloidal suspension was collected separately and centrifuged at 15000 rpm for 30 minutes to retrieve diatom nanoparticles (here named AD-NPs and CAD-NPs). The obtained NPs were subsequently washed in DI water and centrifuge (15000 rpm for 30 minutes) for 3 times to remove any NaOH traces. The settled solid fraction was also collected, re-suspended in DI water and centrifuge as above to recover trapped NPs.

Finally, the remaining settled fraction was collected and washed with DI water to obtain diatom microparticles (named AD-MPs and CAD-MPs, depending on the source of purified diatomite).

2.4 Diatomite, purified diatomite and diatom particles characterization

Composition and mineral contamination of the RD powder , AD and CAD purified powders were characterized by X-ray diffraction (XRD) with a high resolution powder diffractometer (Rigaku PMG/VH, Tokyo, Japan), with Bragg-Brentano geometry in the range 2θ from 5.0 - 60.0 degrees using CuKα radiation (λ =1.5405981 Å). Surface atomic composition of diatomite powders before and after purification was analyzed by X-ray photoelectron spectroscopy (XPS) with a Scienta Gammadata ESCA 200 (Uppsala, Sweden), equipped with monochromatic Al-Kα radiation source (hv = 1486 eV).

A Field-Emission scanning electron microscope (FESEM-Supra 40, Zeiss, Germany) was used for the observation of diatomite powders, diatoms morphology and microparticles size distribution using type II secondary electrons (SE2).

Back scattered electrons (BSE) combined with Energy-Dispersive X-ray analysis (EDAX) were used to detect elemental composition of diatom and contaminations using a FEI/Philips XL30 Environmental Scanning Electron Microscope (ESEM, FEI, Hillsboro, Oregon, USA) equipped with Falcon X-Ray Microanalysis System.

The hydrodynamic radius of diatom NPs in both DI water and PBS was determined by Dynamic Light Scattering (DLS) using a Malvern 110 Zetasizer Nano ZS instrument (Malvern, United Kingdom), equipped with a He–Ne a 5 mW laser at 633 nm). Morphology and chemical analysis of the NPs were also confirmed by transmission electron microscopy with a CM12 TEM, (Philips, Eindhoven, Netherlands) - accelerating voltage 120 KeV - combined with Energy Dispersive X-Ray spectrometer (EXDS).

Surface area and pore size distribution microparticles and nanoparticles were evaluated by physisorption measurements. Nitrogen physisorption experiments were performed at the liquid nitrogen temperature using a Micromeritics ASAP 2010 system (Norcross, GA, USA). All the samples were degassed below 1.3 Pa at 25 °C prior to the measurement. The Specific Surface Area (SSA) values were calculated by the BET equation in the interval $0.05 \leq (p/p_o) \leq 0.33$ [39]. Pore size distribution was calculated using the BJH method applied on both branches of the physisorption isotherms [40].

2.5 Silicon release from diatom particles in DI water

Aliquots of the diatomite-derived NPs and MPs prepared above were dispersed in DI water (100 µg of particles per ml of water) and stored at 37°C to allow for particles dissolution and silicon release. Three replicates for each experimental group (AD-MPs, AD-NPs, CAD-MPs and CAD-NPs) were extracted at predetermined time points (4, 8 and 24 hours; 2, 3, 4, 7 and 14 days). Samples were centrifuged at 15000 rpm for 30 min, and supernatant were collected and stored at –20ºC. Before measurement, the frozen samples were thawed at RT, vortexed and diluted for silicon quantification. Silicon concentration was determined by inductively coupled plasma/optical emission spectroscopy using a Ciros Vision ICP-OES (SPECTRO Analytical Instruments, Germany). A sodium silicate silicate solution (Sigma-Aldrich) was used as standard to build a calibration curve for silicon concentration.

2.6 Cytotoxicity test

Cytotoxicity of diatomite-derived NPs and MPs were performed following the ISO 10993-5 8.3 standard both with direct contact and elution methods. Embryonic Swiss mouse fibroblast cells (3T3) were expanded and cultured at 37ºC with 5% CO_2 in high glucose medium (DMEM) (Euroclone, Pero, Italy), supplemented with 10% fetal bovine serum (Gibco, NY, USA), 2mM L-glutamine, 1mM sodium pyruvate and 0.1% antibiotics (Gibco, NY, USA). The medium was changed every 2 days until cells confluence, then cells were detached with 0.1% trypsin and re-suspended in culture medium. Later, 3T3 cells were plated in polystyrene 48-well plate at a density of 5×10^3 cells/cm^2 and incubated under standard culture conditions.

A reduced culture medium was prepared with Dulbecco's Modified Eagle basal medium without phenol red with 10% heat-inactivated serum, 1 mM sodium pyruvate, 2 mM L-glutamine and 0.1% antibiotics.

Diatom particles (AD-MPs, AD-NPs, CAD-MPs and CAD-NPs) were disinfected with 70% ethanol solution and then collected by centrifugation at 15000 rpm for 30 minutes.

For the evaluation of cytotoxicity in elution mode, diatom particles extracts were prepared by soaking diatom particles in reduced medium for 4 days at 37°C (particles concentration 100, 200, and 500 µg/ml). When cells reached about 70-80% of confluence, culture medium was removed and replaced with conditioned media containing diatom particles extracts. Cells were then cultured in conditioned medium with extracts for 24 hours.

For the evaluation of cytotoxicity in direct contact mode, diatom particles (AD-MPs, AD-NPs, CAD-MPs and CAD-NPs) were directly re-dispersed in reduced medium at designed concentrations (100, 200, and 500 µg/ml). In this mode diatom particles were directly supplied to the cells. 3T3 cells were culture in presence of diatom particles for 24 hours.

Lactate dehydrogenase assay (LDH) (TOX7, Sigma-Aldrich) was used to evaluate the cytotoxicity impact of particles extracts and particles themselves on the cells, following manufacturers' instructions. Cells cultured in reduced medium and treated for 30 min with 0.05% Triton x-100 were used as positive controls. Cell cultured in reduced medium without any diatom sample were used as negative control. Absorbance was measured using a Tecan Infinite 200 microplate reader (Tecan Group, Männedorf, Switzerland) at 490 nm, background absorbance was measured at 690 nm. Results were presented as mean ± standard deviation (n = 5).

3. Results and discussion

3.1 Purification of the raw diatomite powder

Raw diatomite powder (RD) and calcined diatomite powder (CD) were acid-treated with 1M HCl solution to reduce inorganic contaminants.

The yield of the purification process was about 75% in the case of acid-purified diatomite (AD) and 65% for the acid-treated calcined diatomite powder (CAD); that is, 25 to 35 % of the initial RD weight was lost during the different sieving steps, washed away or dissolved during the acidic treatment.

3.2 Characterization of raw diatomite and purified-diatomite

SEM analysis of RD powder revealed whole diatom skeletons surrounded by broken diatom fragments, small aggregates and impurities due to many sources of organic and inorganic contaminations (Figure 1A). In Figure 1B and C it is possible to see that the different sieving steps and the acid treatment significantly reduced diatom fragments and small aggregates both for acid-purified diatomite (AD) and for acid-treated calcined diatomite powder (CAD). However, in both cases it was possible to spot damage diatom skeletons and large diatom fragments.

X-Ray diffraction analysis (Figure 1D) demonstrated the presence of mineral contaminants including illite, halloysite, muscovite, and quartz both in the RD as well as in the purified diatomite powders (AD and CAD). Yet, a reduction of the intensity of the characteristic peaks after purification indicated a decreased amount of quartz and halloysite contaminations (Figure 1D and E).

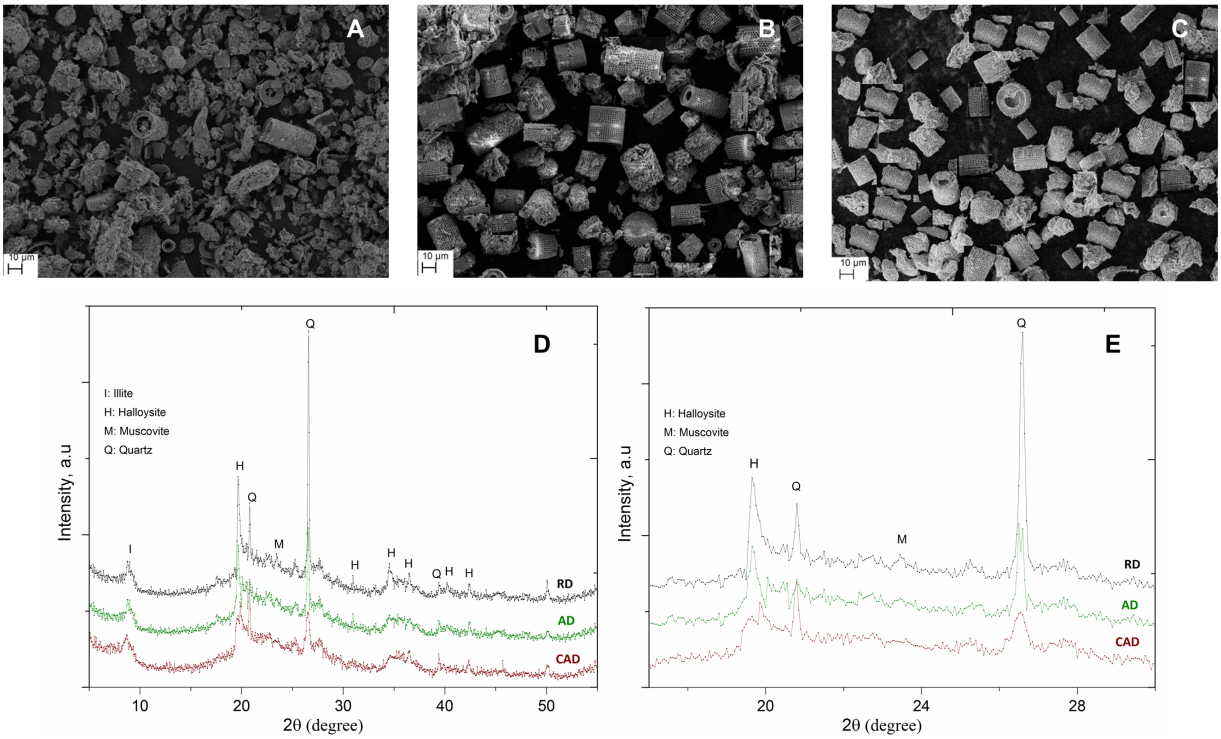

Figure 1: Morphology and mineral composition of raw diatomite (RD) and purified diatomite (AD and CAD) powders. A) SEM micrograph of diatomite powder (RD), B) and C) SEM micrographs of acid-purified raw diatomite (AD) and acid-purified calcined diatomite (CAD), respectively, D) X-Ray spectra of diatomite powders before and after purification showing clay mineral contaminations including illite (I), halloysite (H), muscovite (M)

and crystalline silica (Quartz-Q), E) Detail of the X-Ray spectra in correspondence of the Quartz peak at 2θ = 26.5.

A chemical description of the material surfaces as well as the surface atomic composition of RD powder and purified diatomite powders (AD) and (CAD) were obtained by XPS analysis.

The characteristic wide spectra of diatomite powders (data not shown) established that the surface composition of diatomite powders was formed by a rather rich list of elements. The main elements were oxygen, carbon and silicon, aluminum, iron and magnesium were present to a lower extent. The elements concentrations together with the chemical bond interpretation are summarized in **Errore. L'origine riferimento non è stata trovata.**.

While analyzing the high-resolution spectra of the main component elements, it is possible to understand how the material changes in relation to specific treatments. This is shown in Figure 2 where the C1s core lines of samples RD, AD and CAD are presented. At it can be seen in Figure 2, there is a rather strong change of the core line upon sample treatment. In particular the cleaning procedure leads to a total reduction of the C1s intensity due to the elimination of the main part of the organic contaminants with a significant decrease of the carbon content, from 20.6% to 8.5% and 6.1% in AD and CAD samples, respectively.

In the meanwhile, purified materials AC and CAD resulted to be enriched in silicon, oxygen, aluminum and iron (**Errore. L'origine riferimento non è stata trovata.**).

Also the calcinations processing influenced the C1s line shape. In this case there was an increase of the intensity of the C1s oxidized components which fall in the range 286eV – 290eV for CAD material.

Effect of purifications was mirrored also by the O1s core lines reported Figure 2. The reduction of the hydrocarbon contaminants upon purifications leads to an increase of the total oxygen concentration. Slight decrease of the total oxygen abundance is induced by the calcination in agreement with the decrease of the carbon concentration in the CAD sample.

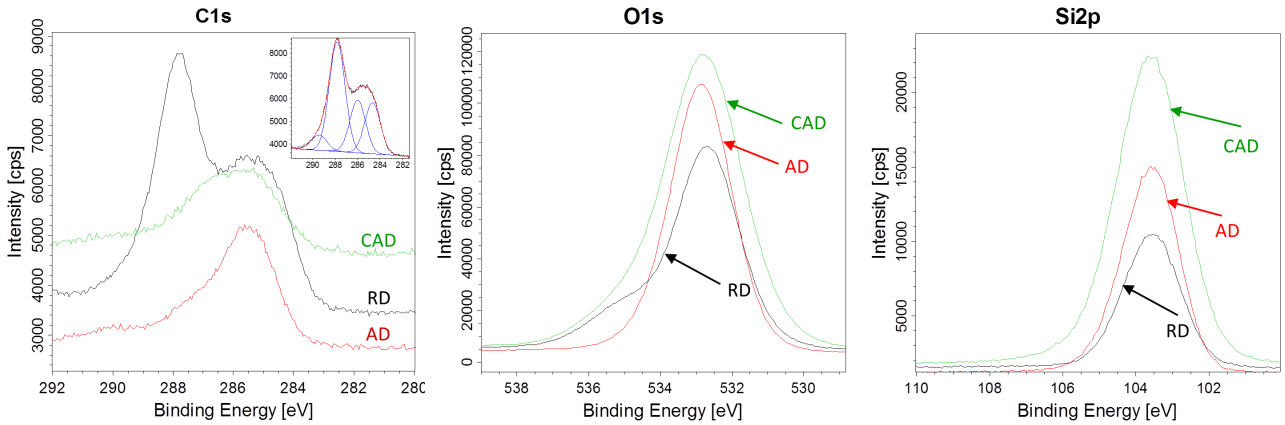

Figure 2: High energy resolution C1s, O1s and Si2p core lines obtained by XPS for raw diatomite powder (RD) and purified diatom powders (AD) and (CAD). In the inset is shown the deconvolution of the C1s core line in Gaussian components. Both purification procedures lead to a drastic reduction of the C1s intensity at 288 eV due to the elimination of the organic contaminants.

As for carbon, also in the case of oxygen sample treatments induce a modulation of the chemical bond intensities. In particular the removing impurities process induces an increase of the intensity of the component associated to the SiO_2 bonds in agreement with the increase of the Si concentration while the component located at high binding energy and associated to H_2O decreases. Also Si2p core line showed a similar trend

(Figure 2). The Si core line was fitted using just one component which represents silicon in SiO_2 chemical configuration. Apart the core line intensity the sample treatments does not have any effect on this chemical bond.

Table 1: Elemental composition of raw diatomite powder (RD) and purified diatomite powders (AD) and (CAD) as determined by X-ray photoelectron spectroscopy (XPS).

Atom %	Si2p	O1s	C1s	Al2p	Fe2p	Mg2p
RD	13.2 ± 1.0	58.9 ±1.7	20.6 ± 1.8	1.7 ± 0.2	2.9 ± 0.2	1.9 ± 0.1
AD	18.4 ± 0.5	62.8 ± 0.6	8.5 ± 0.2	4.7 ± 0.5	4.8 ± 0.4	1.2 ± 0.2
CAD	20.8 ± 0.7	64.0± 0.9	6.1 ± 0.3	4.2 ± 0.3	3.7 ± 0.3	1.6 ± 0.2

While removing small aggregates and diatom fragments, purification processes of RD powder did not change the morphology of diatom skeletons. At the same time, the results from XPS and XRD analyses and SEM observation demonstrated the efficiency of both process of diatomite purifications.

The morphology of single diatom skeletons observed by SEM illustrated the typical morphology of the Aulacoseira diatom group, cylindrical-body shape with diameter of 5 – 20 µm, length of 10– 40 µm, and a wide circular opening on one side (Figure 3). The wall of diatom skeleton presented the typical honeycomb structure, densely populated by pores 400 nm to 800 nm in diameter.

EDAX observation of single diatom skeletons (Figure 3B) indicated the presence of silicon, oxygen, carbon and aluminum, in an agreement with Abramson et al. [4] and Koning et al. [41]. Composition of contaminant particles adhering to the skeleton revealed the presence of iron, potassium and magnesium (Figure 3C).

For a deeper understanding of diatom structure, single skeletons were also investigated by TEM (supplement S1). Diatom skeleton wall revealed rows of aligned nanometric strips of biogenic silica consisting of a regular array of silica nanoparticles. Moreover, biogenic silica strips were organized in lamellar-like structures with different orientations depending on the specific location along the diatom skeleton (supplement S1). Silica nanoparticles deposition and formation of the biogenic silica strip are regulated by the presence of organic molecules [1], thus it could be assumed that association between organic substance and inorganic still remains at the nanoscale on the diatom skeleton structure. This is an agreement with the presence of carbon components in diatom skeleton before and even after purifications (See Table 1).

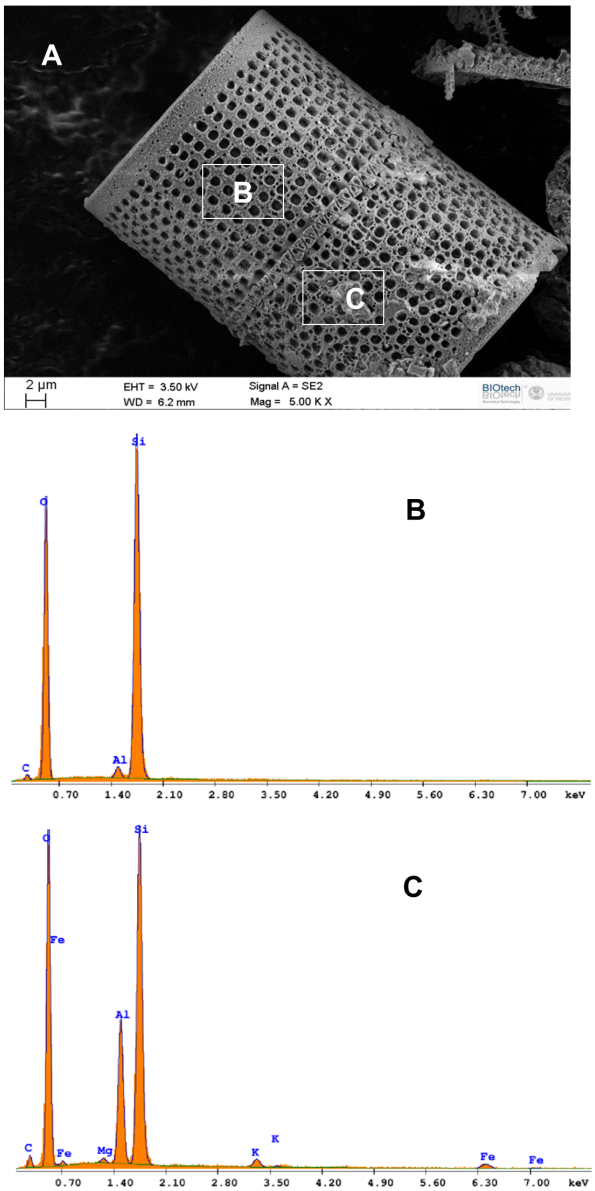

Figure 3: Morphology and elemental composition of diatom skeletons isolated from acid-purified calcined diatoms (CAD) obtained by Energy dispersive X-ray analysis (EDAX). *A) SEM micrograph of a single diatom skeleton, B) elemental composition of the clean diatom wall, C) elemental composition of an impurity/defect of the diatom skeleton. The patterned diatom wall presents a silicon/oxygen composition with low carbon and aluminum content, impurity shows high aluminum content and relevant iron/potassium/magnesium contaminations.*

3.3 Diatomite nanoparticles preparation and morphology

Diatom nanoparticles and microparticles were produced from purified diatomite powders (both AD and CAD) by mechanical fragmentation in alkaline conditions. Nanoparticles were separated by microparticles by sedimentation and recovered from the unsettled colloidal suspension by high speed centrifugation. The yield of the process was around 15% in weight with respect to the weight of purified diatomites (AD and CAD) both for AD-NPs and fro CAD-NPs.

Dynamic light scattering (DLS) demonstrated that purified NPs presented a symmetric broad size distribution both in DI water and PBS, with diameters ranging from 70 to 300 nm, and average size around 170 nm. No statistical differences were found between different samples.

Table 2: Average size of diatom nanoparticles measured by dynamic light scattering (DLS) in DI water and in PBS

Nanoparticles	Average Diameter (nm)	
	DI water	PBS
AD-NPs	171 ± 68	185 ± 66
CAD-NPs	161 ± 79	172 ± 84

TEM micrograph of AD-NPs and CAD-NPs (

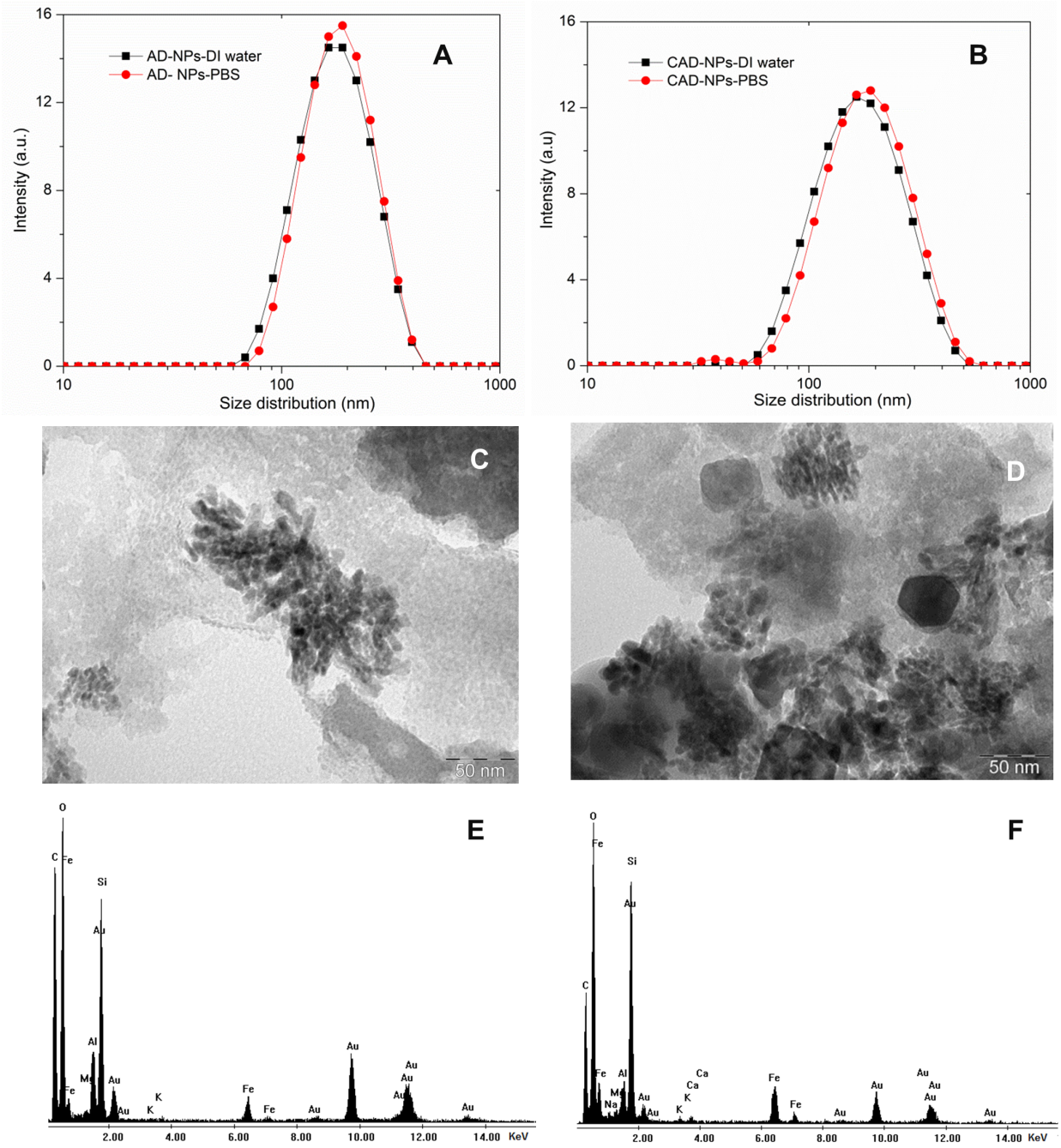

Figure 4C and D) showed irregular particles with a size of 50 nm or more. Interestingly, the irregular particles seemed to be generate by aggregation of smaller biogenic silica nanoparticles about 10 nm in size.

In fact, it is well known that biogenic silica nanoparticles (1 to 10 nm in size) are formed by precipitation of biogenic nanopartilces silica by the action of silaffins in presence of silicic acid and some metallic ions in sea water [1].

These observations are partially in contrast with DLS measurements (Table 2) that demonstrated nanoparticles ranging from 70 to 300 nm. Probably diatom nanoparticles were partially aggregated in DI water as well as in PBS.

EDS spectra for both NPs types showed similar elemental compositions consisting of silicon, oxygen, aluminium and traces of iron and magnesium (

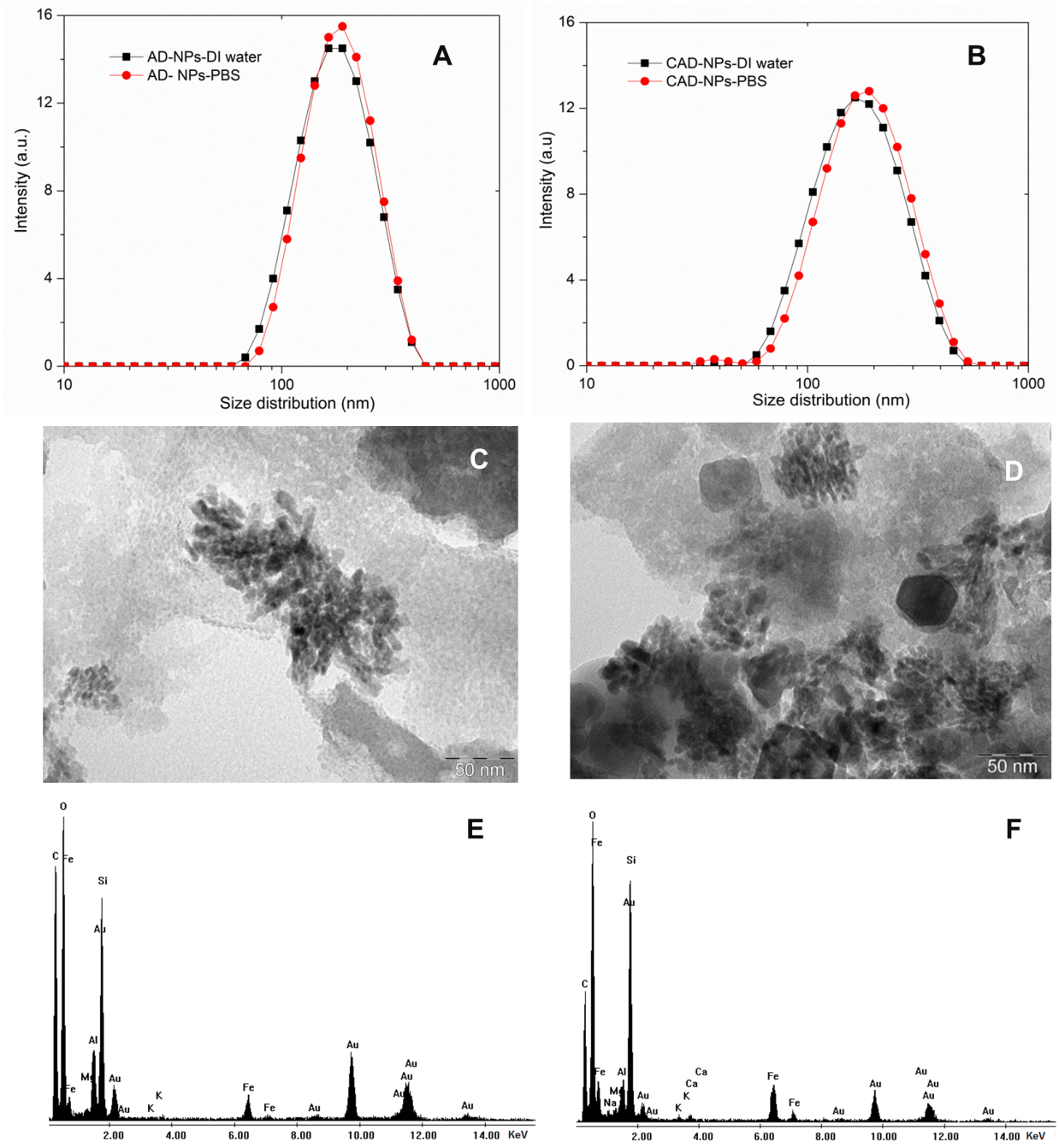

Figure 4E and F). No differences was found about the presence of elemental composition of diatom nanoparticles and diatom skeleton nanostructure (supplement-S1c).

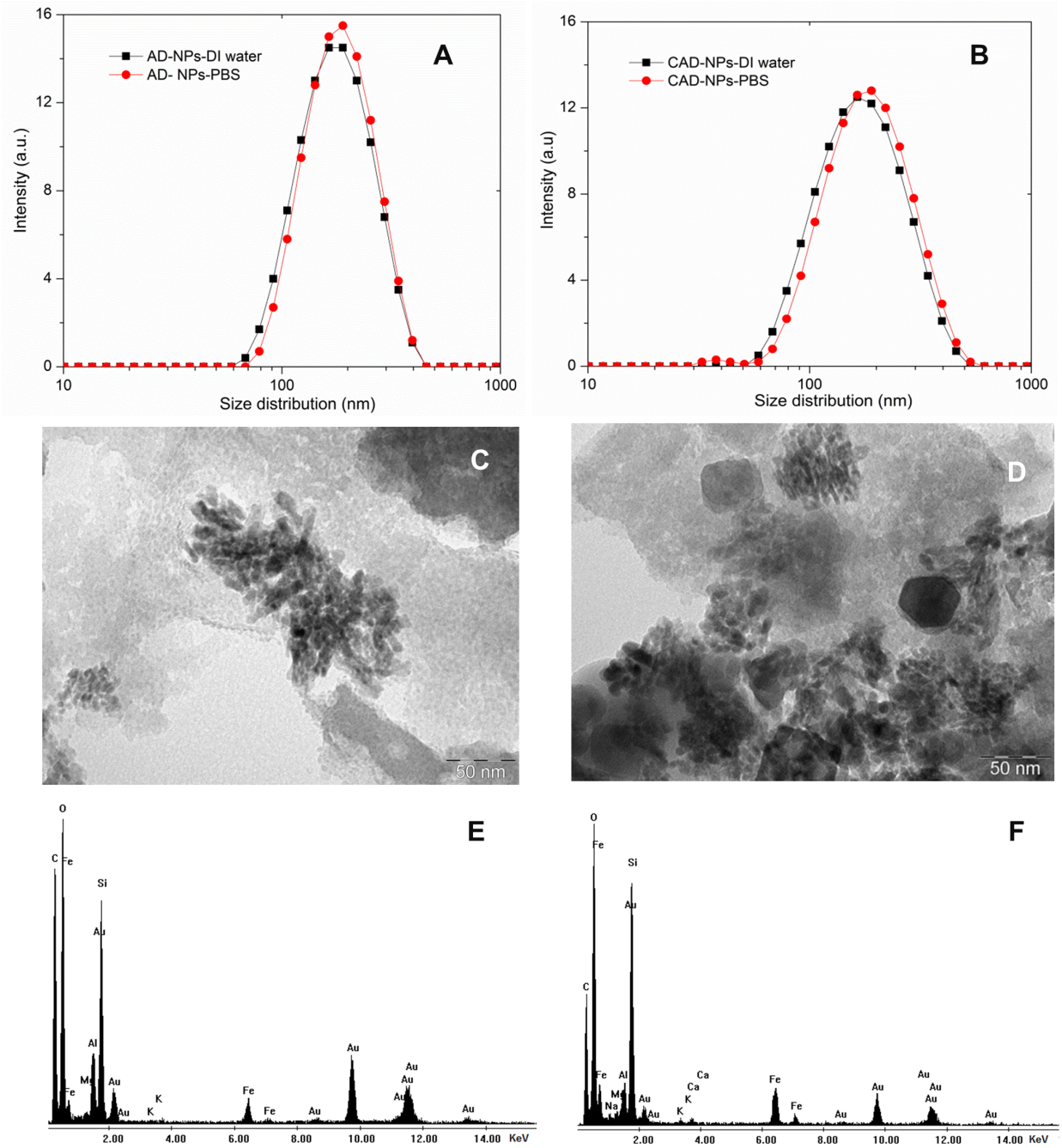

Figure 4: Size distribution, morphology and elemental composition of nanoparticles obtained from acid-purified diatomite (AD-NPs) and acid-purified calcined diatomite (CAD-NPs). A) Size distribution of AD-NPs measured by dynamic light scattering (DLS) in DI water and PBS, B) Size distribution of CAD-NPs, C) and D) TEM micrographs of AD-NPs and CAD-NPs, E) and F) elemental composition of AD-NPs and CAD-NPs determined by EDS. The presence of carbon (E, F) was mainly contributed by ethanol solvent suspended NPs.

Diatom nanoparticles derived from purified diatoms was formed both fragmantation and destructive skeleton by reaction of alumium component under extreme alkaline condition.

The reduction of H_2O at the surface of diatom, the slight changed energy of Si – O based on wider enegry core line of oxygen as well as silicon, and the oxidation of carbon after calcination could be affected resulting NPs composition and also their surface chemical properties.

3.4 Diatoms microparticles morphology

Diatom microparticles were produced from purified diatomite powders (both AD and CAD) and were formed via mechanical fragmentation of diatom skeletons in alkaline conditions. Microparticles were separated by sedimentation and the yield of the process was around 80% in weight with respect to the initial weight of purified diatomites (AD and CAD) both for AD-MPs and fro CAD-MPs. SEM micrographs revealed irregularly-shaped, highly porous MPs with size ranging from 1 to 10 μm (*Figure 5*). Clearly, the MPs consisted of micrometric fragments of skeleton diatom wall; and SEM observation did not show any significant morphological difference between AD-MPs and CAD-MPs.

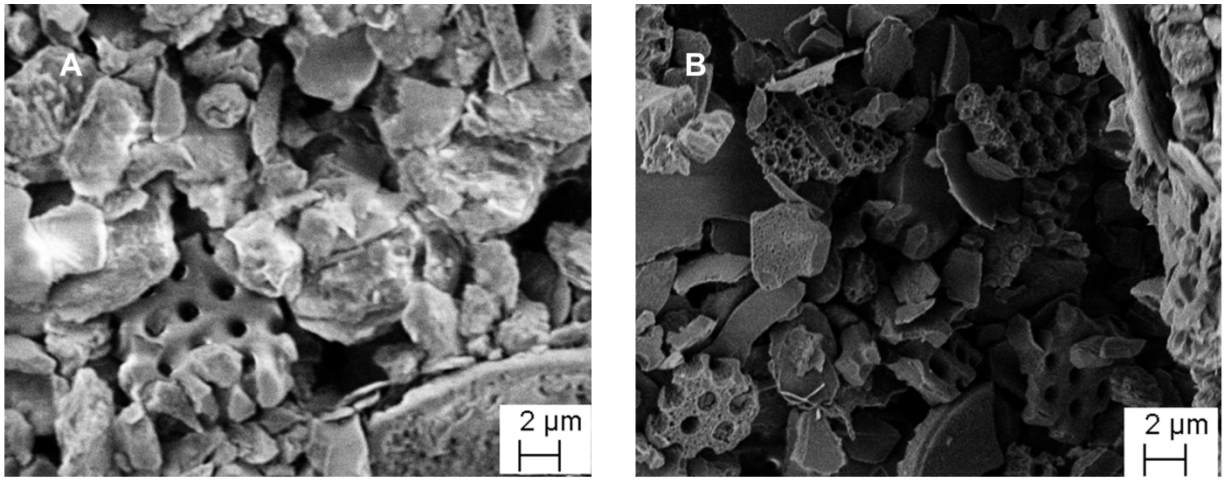

Figure 5: SEM morphology of diatom microparticles. A) Diatom microparticles produced from acid-purified raw diatomite (AD-MPs), B) Diatom microparticles from acid-purified calcined diatomite (CAD-MPs)

3.5 BET surface area of nanoparticles and microparticles

All samples display isotherm curves that can be classified as Type IIb isotherms, according to the IUPAC classification [42] (supplement 2). The presence of a Type H3 hysteresis loop allows to identify the samples as aggregates of plate-like particles with non-rigid slit-shaped pores, whose dimensions fall mainly in the micropore dimensions (< 2 nm in diameter), again according the IUPAC classification. The results are in agreement with those reported in literature for clays [43]. Corresponding surface area values, obtained from BET model, are ranging from 25 m^2/g from diatom AD-MPs to 45 m^2/g for diatom AD-NPs, typical values for this class of solids. Differences between micro- and nano-particle samples can be obtained from the analysis of the derived t-plot, where the adsorbed amount of analysis gas is plotted against the standard multilayer thickness at the corresponding P/P_0 values. Within the limits of this method, pore areas due to the presence of micropores can be determined; as a result, nanoparticle sample displays a higher amount of micropores (about 40% of the whole specific surface area), whereas microparticle one has a lower amount (less than 15% of the whole specific surface area). This result represents the specific feature characterizing different sample; in fact, the pore distribution curves, obtained from BJH method, are quite similar for both samples, as already evidenced by physisorption isotherms, with an approximately monomodal distribution displaying a mode of the curves falling in 2-4 nm diameter range.

BET surface area results, TEM and SEM observations suggest that biogenic silica nanoparticles and microsilica particles were successfully produced from diatom whole skeletons.

3.6 Silicon ion release from dissolution of diatom particles in DI water

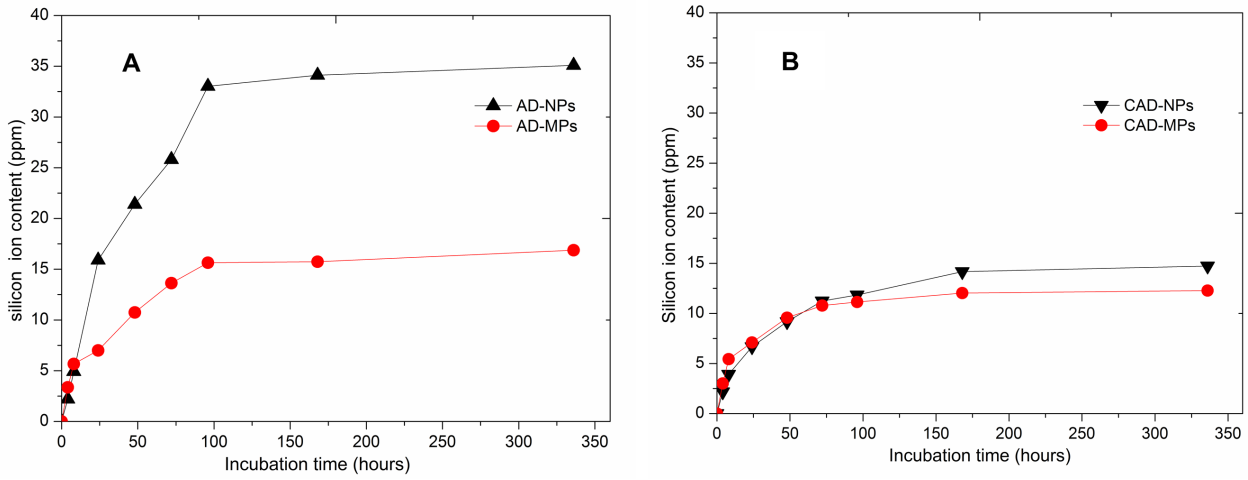

Figure 6: Silicon release profile from diatom nanoparticles and microparticles quantified by inductively couple plasma/optical emission spectroscopy (ICP/OES). A) Particles derived from acid-purified raw diatomite (AD-NPs and AD-MPs), B) Particles derived from acid-purified calcined diatomite (CAD-NPs and CAD-MPs)

The release of silicon ion from diatomite particles dissolution in DI water was determined by ICP/OES analysis of the supernatants.

The kinetics of silicon release from diatoms particles showed an initial fast release followed by a lowering of the rate as the incubation time increased. In particular, in the first 4 days the released silicon ranged from 87% to 92% of its final value.

After 4 days, silicon content, in AD-NPs supernatant was around 3 times higher than in CAD-NPs supernatant (Figure 6), in spite of the comparable silicon content in the two particle groups. Instead, released silicon was 15.6 ppm and 11.1 ppm for AD-MPs and CAD-MPs, respectively.

Nitrogen physisorption analyses determined that diatom NPs presented a specific surface area larger than diatom MPs, and a large part of this difference was related to the contribution of nanosize porosity. Most likely, this difference in surface area between diatom MPs and NPs can partially explain why AD-NPs solubilize faster than AD-MPs.

Solubility of materials based on amorphous biogenic silica has been a controversial topic and a widespread conception [44]. Dissolution can be affected by many experimental factors including solvent characteristics such as ion strength, dissolution temperature and aging mechanisms of the diatomite deposits. DI water was proposed as a suitable model system to assess silica particles solubility and dissolution kinetics [46], [47].

However, dissolution of diatom particles can be influenced by many diatom particles characteristics, such as surface chemistry and structure, morphology, composition and microstructure. For example, the density of hydrophilic silanol groups (-Si-O-H) at the surface of biogenic silica is believed to be an important factor for the control of the dissolution of diatom particles [1].

Zhuravlev [45] found that silanol groups of amorphous silica decreased more than 50 percentage of initial amount after calcination at 600^{0}C. This probably means that the partial removal of hydroxyl group at the surface

of diatoms during to calcination can transform hydrophilic silanol group into hydrophobic siloxanes (≡Si-O-Si ≡) and reduce the density of silanol groups.

As a consequence, different amounts of silanol group at the surface of two types of diatomite NPs could also contribute to explain differences in silicon release kinetics. We suppose that NPs derived from acid-purified raw diatomite should (AD-NPs) presented more surface silanol groups than NPs derived from calcined diatomite (CAD-NPs). For this reason, AD-NPs should dissolve faster than CAD-NPs, thus leading to faster silicon release.

3.7 Cytotoxicity of diatom particles

Toxic effect of diatom particles on 3T3 cells membrane integrity determined the LDH assay showed significant dependence on purifications of diatomite particles and dose of particles. Toxic effect of AD particles was generally larger than CAD particles for both elution and direct method (*Figure 7*). Either no toxicity or negligible toxicity were observed at all concentrations of CAD particles for extract method whilst AD particles showed higher toxicity, especially AD-MPs (*Figure 7*), 5.4% of AD- NPs and 10.6% of AD-NPs respectively.

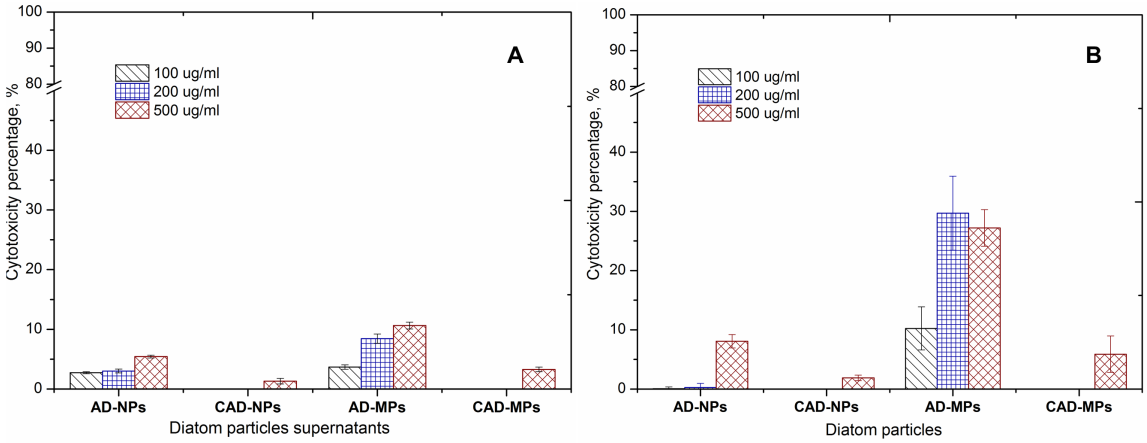

Figure 7: Percentage of cytotoxicity of the different groups of diatom particles on 3T3 cells determined with LDH assay; A) Elution method and B) Direct contact method. Cell cultured in reduced medium without any diatom sample were used as negative control (0% cytotoxicity), while cells treated with 0.05% Triton X-100 surfactant were used as positive control (100% cytotoxicity).

By comparing the results of cytotoxicity from elution method and direct method, no more difference between the cytotoxicity of CAD-NPs performed by extract method and another was found; however, cytotoxicity of CAD-MPs slightly increased at the highest concentration with direct method. Cytotoxicity of AD particles examined by direct method disclosed the increase at the highest concentration, especially AD- MPs (*Figure 7*).

Considering dose dependence, cytotoxicity generally increased following the increase of dose for both NPs and MPs all same concentration.

The presence high silanol groups in AD-supernatant could explain higher toxicity of both AD-NPs and AD-MPs in comparison to CAD-supernatants in the elution mode. Dissolution of possible residual contaminants could also contributed to cytotoxicity of AD samples [18], [48]. Moreover, contact between materials and cells in direct method could be increased their toxic effect on 3T3.

4. Conclusion

In summary, our study has demonstrated the preparation of diatom particles derived from diatom skeletons purified with different purifications of diatomite. Diatom particles could be supposed for bone regenerative application according to silicon release from their dissolution as well as toxic evalution.

The present work compared two different diatomite purifications methods, with and without calcination, and different size diatoms particles derived from, in terms of their element composition, morphology, size and cytotoxic effect on cell cultures. As reported, the two investigated methods resulted in diatoms with different characteristics, mainly in term of composition and stability. Concerning the important role of silicon on the early stage of mineralization, release of silicon from the different types of investigated diatoms fragments has been evaluated. A noticeable effect of the purification method on silicon release and a reduction of silicon release from calcined samples have been demonstrated. Furthermore, we found that diatom-derived particles have limited or no cytotoxic effect in vitro, but purification route could impact the cytotoxicity, especially in the case of microparticles.

The concept of study is due to the introduction of a promising silica source for bone regeneration. Diatoms particles could be used as a supplemental silica materials improving osteoinductive features of natural engineered scaffolds in the future.

Acknowledgements

This study was funded by Erasmus Mundus (2012-2015) project from European commission and Biotech Research Centre, Department of Industrial Engineering, University of Trento, Italy. We are really grateful to prof. Matteo Leoni of University of Trento for XRD analysis.

References

[1] M. Sumper and N. Kröger, “Silica formation in diatoms: the function of long-chain polyamines and silaffins,” *J. Mater. Chem.*, vol. 14, pp. 2059–2065, Jul. 2004.

[2] X. Wang, H. C. Schröder, V. Grebenjuk, B. Diehl-Seifert, V. Mailänder, R. Steffen, U. Schloßmacher, and W. E. G. Müller, “The marine sponge-derived inorganic polymers, biosilica and polyphosphate, as morphogenetically active matrices/scaffolds for the differentiation of human multipotent stromal cells: potential application in 3D printing and distraction osteogenesis,” *Mar. Drugs*, vol. 12, no. 2, pp. 1131–1147, Feb. 2014.

[3] H. C. Schröder, F. Natalio, I. Shukoor, W. Tremel, U. Schlossmacher, X. Wang, and W. E. G. Müller, “Apposition of silica lamellae during growth of spicules in the demosponge Suberites domuncula: biological/biochemical studies and chemical/biomimetical confirmation,” *J. Struct. Biol.*, vol. 159, no. 3, pp. 325–334, Sep. 2007.

[4] L. Abramson, S. Wirick, C. Lee, C. Jacobsen, and J. A. Brandes, “The use of soft X-ray spectromicroscopy to investigate the distribution and composition of organic matter in a diatom frustule and a biomimetic analog,” *Deep Sea Res. Part II Top. Stud. Oceanogr.*, vol. 56, no. 18, pp. 1369–1380, Aug. 2009.

[5] E. M. Carlisle, “Silicon: a possible factor in bone calcification.,” *Science*, vol. 167, no. 3916, pp. 279–80, Jan. 1970.

[6] E. M. Carlisle, “Silicon: A requirement in bone formation independent of vitamin D1,” *Calcif. Tissue Int.*, vol. 33, no. 1, pp. 27–34, Dec. 1981.

[7] E. Bonucci, “The Mineralization of Bone and Its Analogies with Other Hard Tissues,” in *Advanced Topics on Crystal Growth*, S. Ferreira, Ed. InTech, 2013.

[8] K. D. Cashman, “Milk minerals (including trace elements) and bone health,” *Int. Dairy J.*, vol. 16, no. 11, pp. 1389–1398, Nov. 2006.

[9] R. Jugdaohsingh, “Silicon and bone health,” *J. Nutr. Health Aging*, vol. 11, no. 2, pp. 99–110, Jan. 2007.

[10] N. B. Matsko, N. Znidaršič, I. Letofsky-Papst, M. Dittrich, W. Grogger, J. Strus, and F. Hofer, “Silicon: The key element in early stages of biocalcification,” *J. Struct. Biol.*, vol. 174, no. 1, pp. 180–186, Apr. 2011.

[11] S. Heinemann, T. Coradin, and M. F. Desimone, “Bio-inspired silica–collagen materials: applications and perspectives in the medical field,” *Biomater. Sci.*, vol. 1, no. 7, pp. 688–702, Jun. 2013.

[12] S. Amorim, A. Martins, N. M. Neves, R. L. Reis, and R. A. Pires, “Hyaluronic acid/poly- l -lysine bilayered silica nanoparticles enhance the osteogenic differentiation of human mesenchymal stem cells,” *J. Mater. Chem. B*, vol. 2, no. 40, pp. 6939–6946, Aug. 2014.

[13] A. K. Gaharwar, S. M. Mihaila, A. Swami, A. Patel, S. Sant, R. L. Reis, A. P. Marques, M. E. Gomes, and A. Khademhosseini, “Bioactive silicate nanoplatelets for osteogenic differentiation of human mesenchymal stem cells,” *Adv. Mater.*, vol. 25, no. 24, pp. 3329–3336, Jun. 2013.

[14] S. Zou, D. Ireland, R. A. Brooks, N. Rushton, and S. Best, “The effects of silicate ions on human osteoblast adhesion, proliferation, and differentiation,” *J. Biomed. Mater. Res. B. Appl. Biomater.*, vol. 90, no. 1, pp. 123–130, Jul. 2009.

[15] C. T. Price, K. J. Koval, and J. R. Langford, “Silicon: A Review of Its Potential Role in the Prevention and Treatment of Postmenopausal Osteoporosis,” *Int. J. Endocrinol.*, vol. 2013, pp. 1–6, 2013.

[16] Y. F. Zhang, Y. F. Zheng, and L. Qin, “A comprehensive biological evaluation of ceramic nanoparticles as wear debris,” *Nanomedicine*, vol. 7, no. 6, pp. 975–982, Dec. 2011.

[17] A. Tautzenberger, A. Kovtun, and A. Ignatius, “Nanoparticles and their potential for application in bone.,” *Int. J. Nanomedicine*, vol. 7, pp. 4545–57, Jan. 2012.

[18] D. Napierska, L. C. J. Thomassen, D. Lison, J. A. Martens, and P. H. Hoet, “The nanosilica hazard: another variable entity,” *Part. Fibre Toxicol.*, vol. 7, no. 1, pp. 39–71, Jan. 2010.

[19] T.-H. Chung, S.-H. Wu, M. Yao, C.-W. Lu, Y.-S. Lin, Y. Hung, C.-Y. Mou, Y.-C. Chen, and D.-M. Huang, “The effect of surface charge on the uptake and biological function of mesoporous silica nanoparticles in 3T3-L1 cells and human mesenchymal stem cells,” *Biomaterials*, vol. 28, no. 19, pp. 2959–2966, Jul. 2007.

[20] D. M. Brown, N. Kanase, B. Gaiser, H. Johnston, and V. Stone, “Inflammation and gene expression in the rat lung after instillation of silica nanoparticles: effect of size, dispersion medium and particle surface charge,” *Toxicol. Lett.*, vol. 224, no. 1, pp. 147–156, Jan. 2014.

[21] S. Quignard, G. Mosser, M. Boissière, and T. Coradin, “Long-term fate of silica nanoparticles interacting with human dermal fibroblasts,” *Biomaterials*, vol. 33, no. 17, pp. 4431–4442, Jun. 2012.

[22] G. R. Beck, S.-W. Ha, C. E. Camalier, M. Yamaguchi, Y. Li, J.-K. Lee, and M. N. Weitzmann, “Bioactive silica-based nanoparticles stimulate bone-forming osteoblasts, suppress bone-resorbing osteoclasts, and enhance bone mineral density in vivo,” *Nanomedicine nanotechnology, Biol. Med.*, vol. 8, no. 6, pp. 793–803, Aug. 2012.

[23] S.-W. Ha, J. A. Sikorski, M. N. Weitzmann, and G. R. Beck, “Bio-active engineered 50 nm silica nanoparticles with bone anabolic activity: therapeutic index, effective concentration, and cytotoxicity profile in vitro,” *Toxicol. Vitr.*, vol. 28, no. 3, pp. 354–364, Apr. 2014.

[24] I. R. Gibson, S. M. Best, and W. Bonfield, “Chemical characterization of silicon-substituted hydroxyapatite,” *J. Biomed. Mater. Res.*, vol. 44, no. 4, pp. 422–428, Mar. 1999.

[25] W. Xu, C. Ganz, U. Weber, M. Adam, G. Holzhüter, D. Wolter, B. Frerich, B. Vollmar, and T. Gerber, “Evaluation of injectable silica-embedded nanohydroxyapatite bone substitute in a rat tibia defect model,” *Int. J. Nanomedicine*, vol. 6, pp. 1543–52, Jan. 2011.

[26] A. J. Mieszawska, N. Fourligas, I. Georgakoudi, N. M. Ouhib, D. J. Belton, C. C. Perry, and D. L. Kaplan, “Osteoinductive silk-silica composite biomaterials for bone regeneration,” *Biomaterials*, vol. 31, no. 34, pp. 8902–8910, Dec. 2010.

[27] M. L. Foglia, D. E. Camporotondi, G. S. Alvarez, S. Heinemann, T. Hanke, C. J. Perez, L. E. Diaz, and M. F. Desimone, “A new method for the preparation of biocompatible silica coated-collagen hydrogels,” *J. Mater. Chem. B*, vol. 1, no. 45, pp. 6283–6290, 2013.

[28] M. F. Desimone, C. Hélary, I. B. Rietveld, I. Bataille, G. Mosser, M.-M. Giraud-Guille, J. Livage, and T. Coradin, “Silica-collagen bionanocomposites as three-dimensional scaffolds for fibroblast immobilization,” *Acta Biomater.*, vol. 6, no. 10, pp. 3998–4004, Oct. 2010.

[29] I. Izquierdo-Barba, M. Colilla, and M. Vallet-Regí, “Nanostructured Mesoporous Silicas for Bone Tissue Regeneration,” *J. Nanomater.*, vol. 2008, pp. 1–14, 2008.

[30] J. E. N. Dolatabadi and M. de la Guardia, “Applications of diatoms and silica nanotechnology in biosensing, drug and gene delivery, and formation of complex metal nanostructures,” *TrAC Trends Anal. Chem.*, vol. 30, no. 9, pp. 1538–1548, Oct. 2011.

[31] R. Gordon, D. Losic, M. A. Tiffany, S. S. Nagy, and F. A. S. Sterrenburg, “The Glass Menagerie: diatoms for novel applications in nanotechnology,” *Trends Biotechnol.*, vol. 27, no. 2, pp. 116–127, Feb. 2009.

[32] D. Losic, J. G. Mitchell, and N. H. Voelcker, “Diatomaceous Lessons in Nanotechnology and Advanced Materials,” *Adv. Mater.*, vol. 21, no. 29, pp. 2947–2958, Aug. 2009.

[33] M. S. Aw, S. Simovic, Y. Yu, J. Addai-Mensah, and D. Losic, “Porous silica microshells from diatoms as biocarrier for drug delivery applications,” *Powder Technol.*, vol. 223, pp. 52–58, Jun. 2012.

[34] I. Ruggiero, M. Terracciano, N. M. Martucci, L. De Stefano, N. Migliaccio, R. Tatè, I. Rendina, P. Arcari, A. Lamberti, and I. Rea, “Diatomite silica nanoparticles for drug delivery,” *Nanoscale Res. Lett.*, vol. 9, no. 1, pp. 329–336, Jan. 2014.

[35] O. Şan, R. Gören, and C. Özgür, “Purification of diatomite powder by acid leaching for use in fabrication of porous ceramics,” *Int. J. Miner. Process.*, vol. 93, no. 1, pp. 6–10, Sep. 2009.

[36] E. Gulturk, “Thermal and acid treatment of diatom frustules,” *Manuf. Eng.*, vol. 46, no. 2, pp. 196–203, 2011.

[37] H. Ehrlich, K. D. Demadis, O. S. Pokrovsky, and P. G. Koutsoukos, “Modern views on desilicification: biosilica and abiotic silica dissolution in natural and artificial environments,” *Chem. Rev.*, vol. 110, no. 8, pp. 4656–4689, Aug. 2010.

[38] A. Gélabert, O. S. Pokrovsky, J. Schott, A. Boudou, A. Feurtet-Mazel, J. Mielczarski, E. Mielczarski, N. Mesmer-Dudons, and O. Spalla, “Study of diatoms/aqueous solution interface. I. Acid-base equilibria and spectroscopic observation of freshwater and marine species,” *Geochim. Cosmochim. Acta*, vol. 68, no. 20, pp. 4039–4058, Oct. 2004.

[39] S. Brunauer, P. H. Emmett, and E. Teller, “Adsorption of Gases in Multimolecular Layers,” *J. Am. Chem. Soc.*, vol. 60, no. 2, pp. 309–319, Feb. 1938.

[40] E. P. Barrett, L. G. Joyner, and P. P. Halenda, “The Determination of Pore Volume and Area Distributions in Porous Substances. I. Computations from Nitrogen Isotherms,” *J. Am. Chem. Soc.*, vol. 73, no. 1, pp. 373–380, Jan. 1951.

[41] E. Koning, M. Gehlen, A.-M. Flank, G. Calas, and E. Epping, “Rapid post-mortem incorporation of aluminum in diatom frustules: Evidence from chemical and structural analyses,” *Mar. Chem.*, vol. 106, no. 1–2, pp. 208–222, Jul. 2007.

[42] K. S. W. Sing, D. H. Everett, R. A. W. Haul, L. Moscou, R. A. Pierotti, J. Rouquerol, and T. Siemieniewska, “Reporting physisorption data for gas/solid systems with special reference to the determination of surface area and porosity,” *Pure Appl. Chem.*, vol. 57, no. 4, pp. 603–619, Jan. 1985.

[43] S. Kaufhold, R. Dohrmann, M. Klinkenberg, S. Siegesmund, and K. Ufer, “N2-BET specific surface area of bentonites.,” *J. Colloid Interface Sci.*, vol. 349, no. 1, pp. 275–282, Sep. 2010.

[44] R. Viitala, M. Jokinen, S. L. Maunu, H. Jalonen, and J. B. Rosenholm, “Chemical characterization of bioresorbable sol–gel derived SiO2 matrices prepared at protein-compatible pH,” *J. Non. Cryst. Solids*, vol. 351, no. 40–42, pp. 3225–3234, Oct. 2005.

[45] L. T. Zhuravlev, “The surface chemistry of amorphous silica. Zhuravlev model,” *Colloids Surfaces A Physicochem. Eng. Asp.*, vol. 173, no. 1–3, pp. 1–38, Nov. 2000.

[46] J. P. Icenhower and P. M. Dove, “The dissolution kinetics of amorphous silica into sodium chloride solutions: effects of temperature and ionic strength,” *Geochim. Cosmochim. Acta*, vol. 64, no. 24, pp. 4193–4203, Dec. 2000.

[47] C. O. Metin, L. W. Lake, C. R. Miranda, and Q. P. Nguyen, “Stability of aqueous silica nanoparticle dispersions,” *J. Nanoparticle Res.*, vol. 13, no. 2, pp. 839–850, Sep. 2010.

[48] Z. Elias, O. Poirot, I. Fenoglio, M. Ghiazza, M.-C. Danière, F. Terzetti, C. Darne, C. Coulais, I. Matekovits, and B. Fubini, “Surface reactivity, cytotoxic, and morphological transforming effects of diatomaceous Earth products in Syrian hamster embryo cells,” *Toxicol. Sci.*, vol. 91, no. 2, pp. 510–520, Jun. 2006.